Atmospheric Environment 59 (2012) 170–185

Contents lists available at SciVerse ScienceDirect

Atmospheric Environment

journal homepage: www.elsevier.com/locate/atmosenv

Simulation of the interannual variations of biogenic emissions of volatile organic compounds in China: Impacts on tropospheric ozone and secondary organic aerosol

Yu Fu [a,b], Hong Liao [a,*]

[a] State Key Laboratory of Atmospheric Boundary Layer Physics and Atmospheric Chemistry (LAPC), Institute of Atmospheric Physics, Chinese Academy of Sciences, Beijing 100029, China
[b] Graduate University of Chinese Academy of Sciences, Beijing 100049, China

HIGHLIGHTS

- We have updated land cover and leaf area index in China in MEGAN to estimate BVOCs.
- Simulated isoprene emissions in China have large interannual variations of 15–42%.
- Simulated monoterpene emissions in China have large interannual variations of 10–32%.
- Interannual variations of BVOCs can lead to 2–5% differences in O_3 and SOA in July.

ARTICLE INFO

Article history:
Received 10 March 2012
Received in revised form
24 May 2012
Accepted 30 May 2012

Keywords:
Biogenic emissions
Tropospheric ozone
Secondary organic aerosol
Interannual variations

ABSTRACT

We use the MEGAN (Model of emissions of Gases and Aerosols from Nature) module embedded within the global three-dimensional Goddard Earth Observing System chemical transport model (GEOS-Chem) to simulate the interannual variations in biogenic volatile organic compound (BVOC) emissions and concentrations of ozone and secondary organic aerosols (SOA) in China over years 2001–2006. To have better representation of biogenic emissions, we have updated in the model the land cover and leaf area index in China using Moderate Resolution Imaging Spectroradiometer (MODIS) satellite measurements, and we have developed a new classification of vegetation with 21 plant functional types. Estimated annual BVOC emission in China averaged over 2001–2006 is 18.85 Tg C yr^{-1}, in which emissions of isoprene, monoterpenes, and other reactive volatile organic compounds account for 50.9%, 15.0%, and 34.1%, respectively. The simulated BVOC emissions in China have large interannual variations. The values of regionally averaged absolute percent departure from the mean (APDM) of isoprene emissions are in the range of 21–42% in January and 15–28% in July. The APDM values of monoterpene emissions are 14–32% in January and 10–21% in July, which are generally smaller than those of isoprene emissions. Model results indicate that the interannual variations in isoprene emissions are more dependent on variations in meteorological fields, whereas the interannual variations in monoterpene emissions are more sensitive to changes in vegetation parameters. With fixed anthropogenic emissions, as a result of the variations in both meteorological parameters and vegetation, simulated O_3 concentrations show interannual variations of 0.8–5 ppbv (or largest APDM values of 4–15%), and simulated SOA shows APDM values of 5–15% in southwestern China in January as well as 10–25% in southeastern and 20–35% in northeastern China in July. On a regional mean basis, the interannual variations in BVOCs alone can lead to 2–5% differences in simulated O_3 and SOA in summer.

1. Introduction

Volatile organic compounds (VOCs) in the atmosphere are important for air quality and climate. Biogenic isoprene (C_5H_8), alkenes, and acetone are important precursors of tropospheric O_3 (Arneth et al., 2011), and biogenic isoprene and monoterpenes ($C_{10}H_{16}$) are major sources of secondary organic aerosols (SOA) (Carslaw et al., 2010; Nozière et al., 2011). Ozone and SOA are both air pollutants that can influence the Earth's radiation budget (IPCC, 2007). Biogenic emissions of VOCs have been estimated to be equal to or exceed anthropogenic emissions on a global scale. The global

* Corresponding author.
E-mail address: hongliao@mail.iap.ac.cn (H. Liao).

1352-2310/$ – see front matter © 2012 Elsevier Ltd. All rights reserved.
http://dx.doi.org/10.1016/j.atmosenv.2012.05.053

annual biogenic emission of isoprene was estimated to be in the range of 400–600 Tg C (Arneth et al., 2008) and that of monoterpenes was estimated to be 33–147 Tg C yr^{-1} (Guenther et al., 1995, 2006; Heald et al., 2008; Schurgers et al., 2009). Over China, the annual isoprene and monoterpene emissions were estimated to be in the ranges of 4.1–15.0 Tg C and 3.5–6.0 Tg C (Klinger et al., 2002; Steiner et al., 2002), respectively.

Biogenic emissions have been shown to have large interannual variations. Tsigaridis et al. (2005) estimated that the annual and global BVOC emission could differ by 7% during years 1984–1993 as a result of the changes in meteorological variables. Lathiere et al. (2006) found that, relative to the averaged biogenic emission over 1983–1995, annual isoprene emission over the studied period varied in the range of −11.5% to +6.8% in Europe and by about ±10% in North and South America and Africa, mainly because of the variations in air temperature. Arneth et al. (2011) found that the interannual variations in isoprene emission are the largest (up to 15%) in the northern high latitudes (60°–90°N), because the variations in gross primary productivity or LAI of the major emitting plant functional types (PFTs) are the more significant in 60°–90°N than in other regions.

Biogenic emissions of isoprene and monoterpenes are also shown to have large variations on decadal to centennial time scales, as a result of the changes in both vegetation and climate. With fixed vegetation, studies that considered different scenarios of future climate predicted increases in global biogenic emission of 22–55% from present day to 2100 (Heald et al., 2008; Liao et al., 2006; Wu et al., 2012). Because of the simulated climate-induced large expansion of temperate and boreal broadleaved forests in high latitudes in 2100, the year 2100 global biogenic emission of isoprene simulated with present-day climate and future vegetation was found to be higher by about 25% than that simulated with present-day climate and vegetation, when the future impact of CO_2 on vegetation was considered (Wu et al., 2012). Anthropogenic land use changes were predicted to reduce the global isoprene emission by 15% over 1901–2002 as a result of the anthropogenic cropland expansion (Lathière et al., 2010).

The changes in biogenic emissions on interannual, decadal, and centennial time scales can influence concentrations of tropospheric O_3. Curci et al. (2009) used a regional air quality model to investigate the surface-layer O_3 concentrations over Europe in April–September for 4 years (1997, 2000, 2001, 2003), and found that the O_3 concentrations averaged inland can differ by 0.8 ppbv as a result of the interannual variations in meteorological parameters and hence in BVOC emissions. Jiang et al. (2008) investigated the effects of climate and land use changes over 2001–2051 on surface O_3 concentrations in Houston, Texas under the IPCC A1B scenario (the A1B scenario represents rapid growth with low population growth and rapid introduction of new and more efficient technology). They found that over 2001–2051 the daily maximum 8-h O_3 concentrations increase by 2.6 ppbv as a result of the future climate change and the climate-induced increases in BVOCs. On a centennial time scale, Sanderson et al. (2003) reported that the surface-layer O_3 concentrations in July can increase by 20–30 ppbv owing to the increases in anthropogenic precursors from 1990s to 2090s when vegetation was fixed, but only by 10–20 ppbv if vegetation changes in the same period were considered. The changes in BVOCs can either increase or reduce regional O_3 concentrations depending on the regional NO_x/VOC ratios (Wiedinmyer et al., 2006).

The impact of the variations in biogenic emissions on concentrations of SOA depends on POA (on which SOA condenses on) concentrations and regional meteorological conditions. Liao et al. (2006) predicted an increase in global SOA burden from 0.35 Tg in year 2000 to 0.38 Tg in 2100 as a result of the CO_2-induced climate change and a corresponding 55% increase in global biogenic emission under the IPCC A2 scenario, as anthropogenic emissions were fixed at the year 2000 levels. Kanakidou and Tsigaridis (2007) found a two-fold increase in year 2100 SOA burden when the simulation with 2100 climate and 2100 BVOCs was compared to that with 2100 climate and 1990 BVOCs. Heald et al. (2008) reported that, relative to SOA in present day, the anthropogenic land use changes over 2000–2100 following the IPCC A1B scenario alone can reduce the global annual mean SOA burden by 14%. These studies indicate that the anthropogenic land use and climate-driven changes in vegetation have opposing influences on SOA concentrations.

The aforementioned studies underscored the important impacts of the changes in BVOCs on regional O_3 and SOA, but those studies were mostly focused on Europe and the United States. Previous studies that investigated the roles of biogenic emissions in O_3 formation in China were primarily trying to quantify the differences in simulated O_3 concentration with and without biogenic emissions (Geng et al., 2011; Han et al., 2005; Lin et al., 2008), which reported that biogenic emissions can increase O_3 concentrations by 5–30 ppbv because most industrialized regions in China are VOCs-limited. No previous studies, to our knowledge, have examined the interannual variations in BVOCs and their impacts on O_3 and SOA concentrations in China.

We examine in this work the interannual variations in biogenic emissions resulted from the changes in meteorological condition and/or land cover during 2001–2006, using the MEGAN (Model of emissions of Gases and Aerosols from Nature) module embedded within the global three-dimensional chemical transport model GEOS-Chem. To have better representation of the interannual variations of vegetation in China, we have updated the land cover and leaf area index in the model using the MODIS satellite measurements and developed a new classification of vegetation with 21 plant functional types to consider different climatological conditions in China. We examine the key parameters that influence the interannual variations of BVOCs, and then quantify how these interannual variations in BVOCs influence O_3 and SOA concentrations in China.

Section 2 describes the model, the updates in representation of land cover and biogenic emissions, and then the numerical experiments. In Section 3 we present simulated distributions and seasonal to interannual variations in biogenic emissions in China. The simulated interannual variations in concentrations of O_3 and SOA are shown in Sections 4, and the impacts of the interannual variations in BVOC emissions on O_3 and SOA are examined in Section 5.

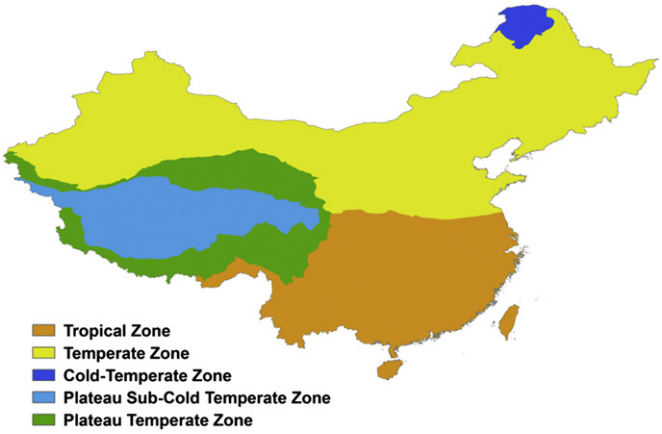

Fig. 1. Typical climatological zones in China.

Table 1
Isoprene and monoterpenes emission factors and specific leaf weight (SLW) used in this study.

Climatic zone	Plant functional types (PFTs)	Emission factors (E_{fi}, μg C gdm^{-1} h^{-1})		SLW[a] (s_i) (gdm m^{-2})	References[b]
		Isoprene	Monoterpenes		
Cold-temperate	1 Evergreen needleleaf trees	8	2.4	150	1,2
	2 Deciduous needleleaf trees	8	2.4	150	2
	3 Deciduous broadleaf trees	8	2.4	150	2
Temperate	4 Evergreen needleleaf trees	16	2.4	150	1
	5 Deciduous needleleaf trees	8	0.8	150	1,3
	6 Deciduous broadleaf trees	45	1.2	100	1,2
Tropical	7 Evergreen needleleaf trees	24	0.8	125	1,2
	8 Deciduous needleleaf trees	24	0.8	125	1,2
	9 Deciduous broadleaf trees	24	0.8	125	3
	10 Evergreen broadleaf trees	24	0.8	125	3
Plateau temperate	11 Evergreen needleleaf trees	16	2.4	150	1
	12 Evergreen broadleaf trees	16	0.8	125	1
	13 Deciduous needleleaf trees	8	2.4	150	2
	14 Deciduous broadleaf trees	45	0.8	100	2
Plateau sub-cold temperate	15 Evergreen needleleaf trees	8	2.4	150	1
	16 Deciduous broadleaf trees	8	1.2	125	1
	17 Shrub	20	0.8	125	1
	18 C_3 Grass	5	0.8	125	2,4
	19 C_3 & C_4 Grass	5	1.2	125	2,4
	20 Cereal crops	5	0.2	125	2
	21 Broadleaf crops	5	0.2	125	2
	22 Urban and built-up	0	0	0	–
	23 Snow and ice	0	0	0	–
	24 Barren or sparse vegetation	0	0	0	–
	25 Water	0	0	0	–

[a] SLW: Leaf dry weight per unit leaf area (gdm m^{-2}), which is the inverse of specific leaf area (SLA, m gdm^{-2}).
[b] 1 Guenther et al. (1995); 2 Lathiere et al. (2006); 3 Levis et al. (2003); 4 Bai et al. (2006).

2. Model description and numerical experiments

2.1. GEOS-Chem

We simulate biogenic emissions and concentrations O_3 and SOA using the global three-dimensional chemical transport model GEOS-Chem (version 8-03-02, http://acmg.seas.harvard.edu/geos/geos_chem_narrative.html) driven by the assimilated meteorological data from the Goddard Earth Observing System (GEOS) of the NASA Global Modeling and Assimilation Office. The version of the model we use is driven by the GEOS-4 meteorological fields with a horizontal resolution of 2° latitude by 2.5° longitude and 30 vertical layers up to 0.01 hPa.

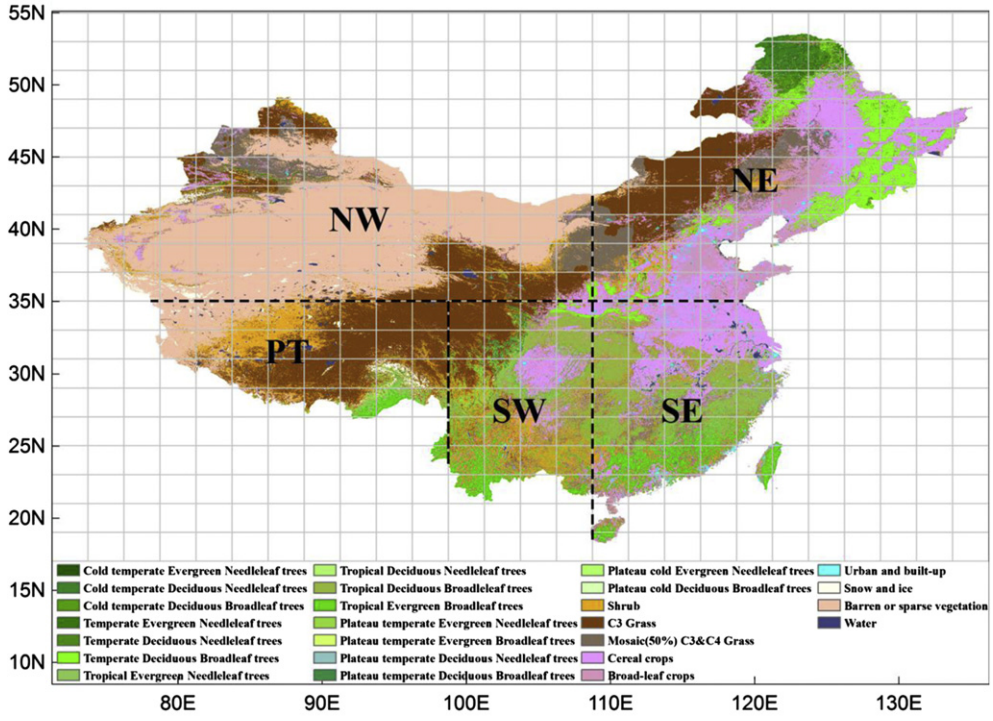

Fig. 2. The distribution of plant functional types (PFTs) in China in year 2003. The regions of China examined in this study are also shown, including northeastern (NE, 35.00°–53.00°N, 108.75°–136.25°E), southeastern (SE, 17.00°–35.00°N, 108.75°–123.75°E), northwestern (NW, 35.00°–49.00°N, 73.75°–108.75°E), southwestern (SW, 21.00°–35.00°N, 96.25°–108.75°E), and plateau (PT, 27.00°–35.00°N, 76.25°–98.75°E) regions.

Table 2
Summary of the GEOS-Chem simulations in this study.

Simulation	MODIS vegetation parameters	GEOS-4 meteorology parameters	BVOC emissions		Simulated O_3 and SOA concentrations
			Calculated online using MEGAN	Monthly BVOCs from ANNmet	
ANNall	2001–2006	2001–2006	2001–2006	–	2001–2006
ANNmet	2003	2001–2006	2001–2006	–	2001–2006
ANNveg	2001–2006	2003	2001–2006	–	2001–2006
ANNmet_ATM	2003	2001–2006	–	2003	2001–2006
ANNmet_BVOCs	2003	2003	–	2001–2006	2001–2006

The GEOS-Chem model has fully coupled ozone-NO_x-VOC-hydrocarbon chemistry and aerosol components including sulfate (SO_4^{2-})/nitrate (NO_3^-)/ammonium (NH_4^+) (Park et al., 2004; Pye et al., 2009), organic carbon (OC) and black carbon (BC) (Park et al., 2003), sea salt (Alexander et al., 2005), and mineral dust (Fairlie et al., 2007). Tropospheric ozone is simulated with about 80 species and over 300 chemical reactions (Bey et al., 2001). SOA formation considers the oxidation of isoprene (Henze and Seinfeld, 2006), monoterpenes and other reactive VOCs (ORVOCs) (Liao et al., 2007), and aromatics (Henze et al., 2008). Wet deposition scheme in GEOS-Chem is described by Liu et al. (2001). The dry deposition velocities are calculated locally dependent on species properties, surface type, and meteorological condition. To see the impacts of biogenic emissions on simulated O_3 and SOA, the Olson land cover classes (Olson, 1992) are used to calculate dry deposition and are assumed not to change in this study.

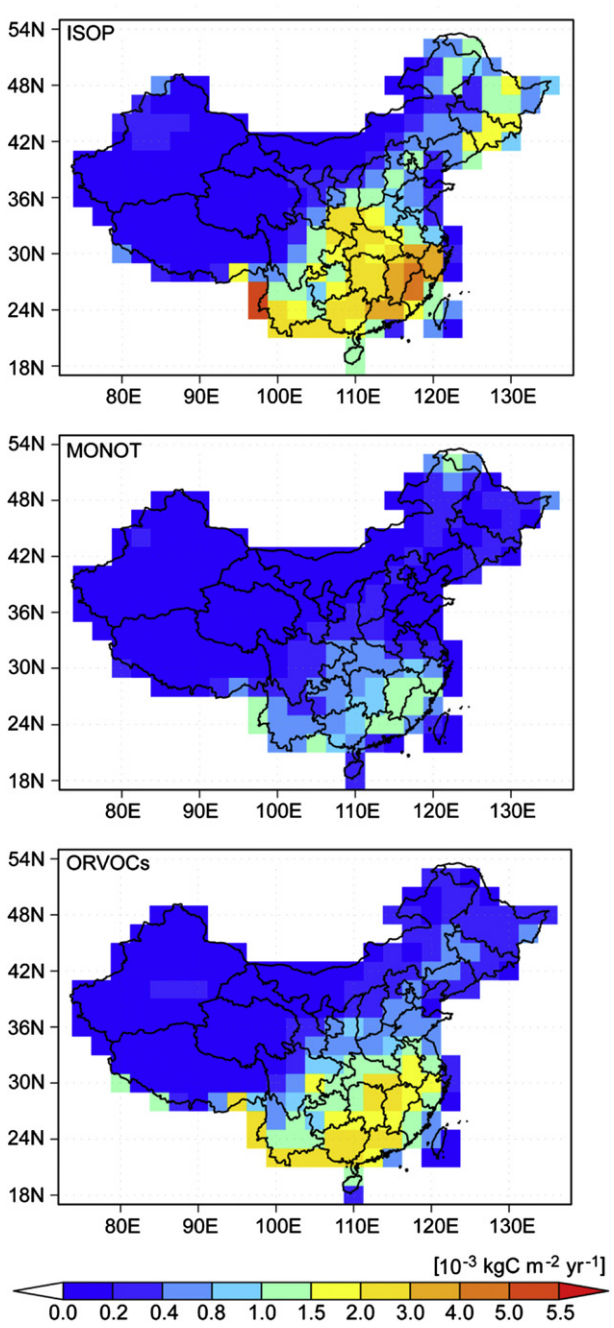

Fig. 3. Simulated annual biogenic emissions (10^{-3} kg C m^{-2} yr^{-1}) of isoprene, monoterpenes, and ORVOCs averaged over years 2001–2006 of simulation ANNall.

Global emissions of ozone precursors, aerosol precursors, and aerosols in GEOS-Chem are taken from the EDGAR 3.2 global inventory for 2000 (Olivier and Berdowski, 2001), while anthropogenic emissions of nonmethane VOCs are from the GEIA inventory for 1985 (Piccot et al., 1992). These default inventories are then scaled for subsequent years on the basis of economic data. In this study, the anthropogenic emissions of SO_2, CO, NO_x, BC, and OC in Asian domain are replaced by those in David Streets' 2006 emission inventory (Streets et al., 2006).

2.2. Vegetation from the MODIS

2.2.1. Vegetation classifications

We develop the land cover data for China using the MODIS derived high resolution (500-m) land cover product from 2001 to 2006 (MCD12Q1, https://lpdaac.usgs.gov/lpdaac/products/modis_products_table/). This product has multiple land cover classification schemes from the remote sensing analysis of Terra and Aqua satellite data (Friedl et al., 2010). Here we choose the classification with 12 plant functional types, including 9 natural vegetation classes (evergreen needleleaf trees, evergreen broadleaf trees, deciduous needleleaf trees, deciduous broadleaf trees, shrub, grass, cereal crops, broadleaf crops, barren and sparse vegetation) and 3 non-vegetated land types (water, urban and built-up, snow and ice). For evergreen needleleaf trees, evergreen broadleaf trees, deciduous needleleaf trees, and deciduous broadleaf trees, we classify them further according to five typical climatological conditions (tropical, temperate, cold-temperate, plateau temperate, and plateau sub-cold temperate climatic zones) in China (Fig. 1). The climate zones are obtained based on the observed temperature and precipitation datasets at 752 weather stations in China in years 1971–2000 (http://cdc.cma.gov.cn/), following the standards of regionalization in China-climatic zones

Table 3
Simulated BVOC emissions averaged over 2001–2006 for different regions (Tg C yr^{-1}).

	China	NE	NW	SE	SW	Plateau
Isoprene	9.59	1.78	0.29	4.54	2.75	0.23
Monotepernes	2.83	0.54	0.13	1.20	0.81	0.15
ORVOCs	6.43	0.87	0.24	2.88	2.01	0.43
Total BVOCs	18.85	3.19	0.66	8.62	5.57	0.81

and climatic regions (CNIS, 1998). As to grass, we classify it as types of C_3 and mosaic with 50% C_4 and 50% C_3, following the rules of Bonan et al. (2002). Crops are classified as cereal and broadleaf crops. As a result, we consider 21 types of vegetation and 4 types of non-vegetated land (urban and built-up, snow and ice, barren land, and water) in this study. Table 1 lists all the 25 land cover types and Fig. 2 shows the distribution of our newly classified PFTs in China in year 2003.

2.2.2. Leaf area index (LAI)

The datasets of LAI ($m^2\ m^{-2}$) in China for years 2001–2006 are obtained from the MODIS products (MOD15A2 version 5, https://lpdaac.usgs.gov/lpdaac/products/modis_products_table/) of monthly mean leaf area index with resolutions of 8 day and 1 km. This LAI product is derived from the spatial averages of the MODIS TERRA satellite images, which has been evaluated against field campaigns (Myneni et al., 2002). The monthly mean LAI is then averaged over the fraction of land area covered by vegetation within the grid cell (referred to as LAIv). The values of LAIv are assumed not to exceed 6 $m^2\ m^{-2}$ as suggested by Guenther et al. (2006).

2.3. Simulation of biogenic emissions

The biogenic emissions in the GEOS-Chem model are simulated using the MEGAN module (Guenther et al., 2006; Wiedinmyer et al., 2007). In the version of the model we use, biogenic emissions of 12 chemical species are simulated, including isoprene, monoterpenes (α-pinene, β-pinene, limonene, myrcene, sabinene, 3-carene, and ocimene), methyl-butenol (MBO), acetone, and the lumped >=C3 alkenes. The emissions, E, of these compounds are determined by

$$E = E_0 \times \gamma_{CE} \times \gamma_{age} \times \gamma_{SM} \times \rho \quad (1)$$

where E_0 ($\mu g\ C\ m^{-2}\ h^{-1}$) is the emission factor which represents the emission of a compound into the canopy at standard conditions (air temperature = 303 K, photosynthetic active radiation (PAR) = 1500 $\mu mol\ m^{-2}\ s^{-1}$, LAI = 5 $m^2\ m^{-2}$), which is multiplied by emission activity factors that represent changes in the emission rate attributing to the changes in the canopy environment γ_{CE}, leaf age γ_{age}, and soil moisture γ_{SM}. We do not consider the effect of soil moisture and the extra production or loss of BVOCs in the

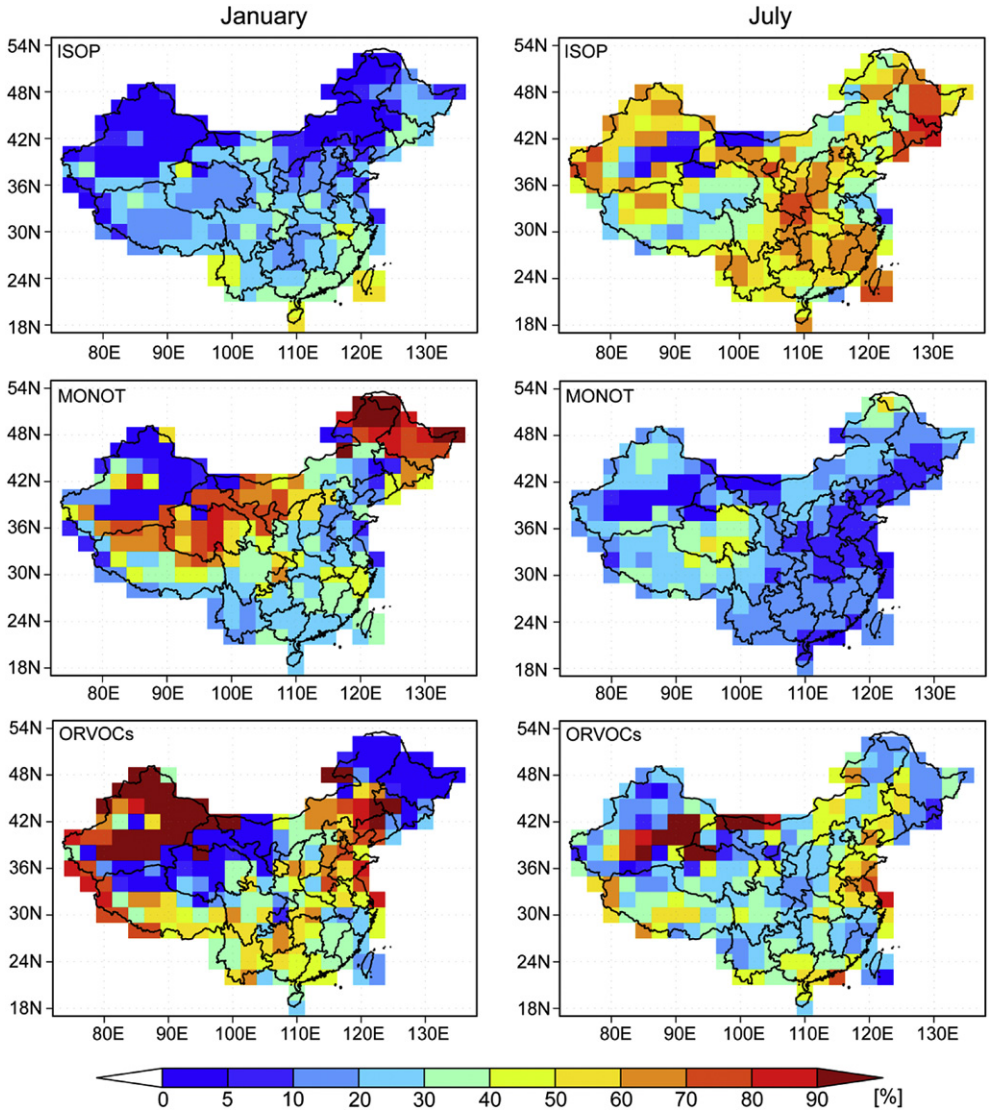

Fig. 4. Ratios of emissions of isoprene, monoterpenes, and ORVOCs to total BVOC emission for January (left column) and July (right column). Emissions are obtained from simulation ANNall and averaged over 2001–2006.

vegetation canopy in this work by setting $\gamma_{SM} = 1$ and $\rho = 1$. γ_{CE} is a function of temperature, PAR, and LAI, which is parameterized differently for different biogenic species (Guenther et al., 2006).

The emission factor E_0 of a biogenic compound (for example, isoprene or monoterpenes) in each gird cell is calculated as

$$E_0 = \sum_{i=1}^{n} E_{fi} \times s_i \times \omega_i \quad (2)$$

where E_{fi} (μg C gdm^{-2} h^{-1}) is the specific emission factor prescribed for the ith PFT in the grid cell under standard conditions, s_i (gdm m^{-2}, dm represents dry matter) is the specific leaf weight of the ith PFT, and ω_i is the fraction of the grid area covered by the ith PFT. The values of E_{fi} and s_i for the improved PFT types in this work are taken from the literature and shown in Table 1.

The only ORVOC species that is predicted in GEOS-Chem/MEGAN is MBO. To account for SOA formation from ORVOCs including sesquiterpenes, we use the monthly ORVOC emissions from the Global Emissions Inventories Activity (GEIA) as in Liao et al. (2007). The interannual variation of ORVOCs in a grid cell is scaled by the simulated interannual variation in emissions of MBO.

2.4. The simulations

We perform the following simulations using GEOS-Chem/MEGAN to examine the land cover and/or meteorological changes that influence the interannual variations of BVOCs and concentrations of O_3 and SOA over 2001–2006 (Table 2):

(1) ANNall: The control simulation of biogenic emissions and concentrations of O_3 and SOA for years 2001–2006 with interannual variations in both meteorological and vegetation parameters.
(2) ANNmet: The simulation to examine how BVOC emissions and concentrations of O_3 and SOA are influenced by the interannual variations of meteorological parameters. Meteorological fields are allowed to change from 2001 to 2006. Vegetation parameters (LAIv and PFTs) are kept at the year 2003 values, and the BVOC emissions estimated using the MEGAN module can still vary with meteorological parameters.
(3) ANNveg: The simulation to examine how BVOC emissions and concentrations of O_3 and SOA are influenced by interannual variations in vegetation parameters (LAIv and PFT) over 2001–2006. Year 2003 meteorological fields are used to drive the GEOS-Chem/MEGAN.

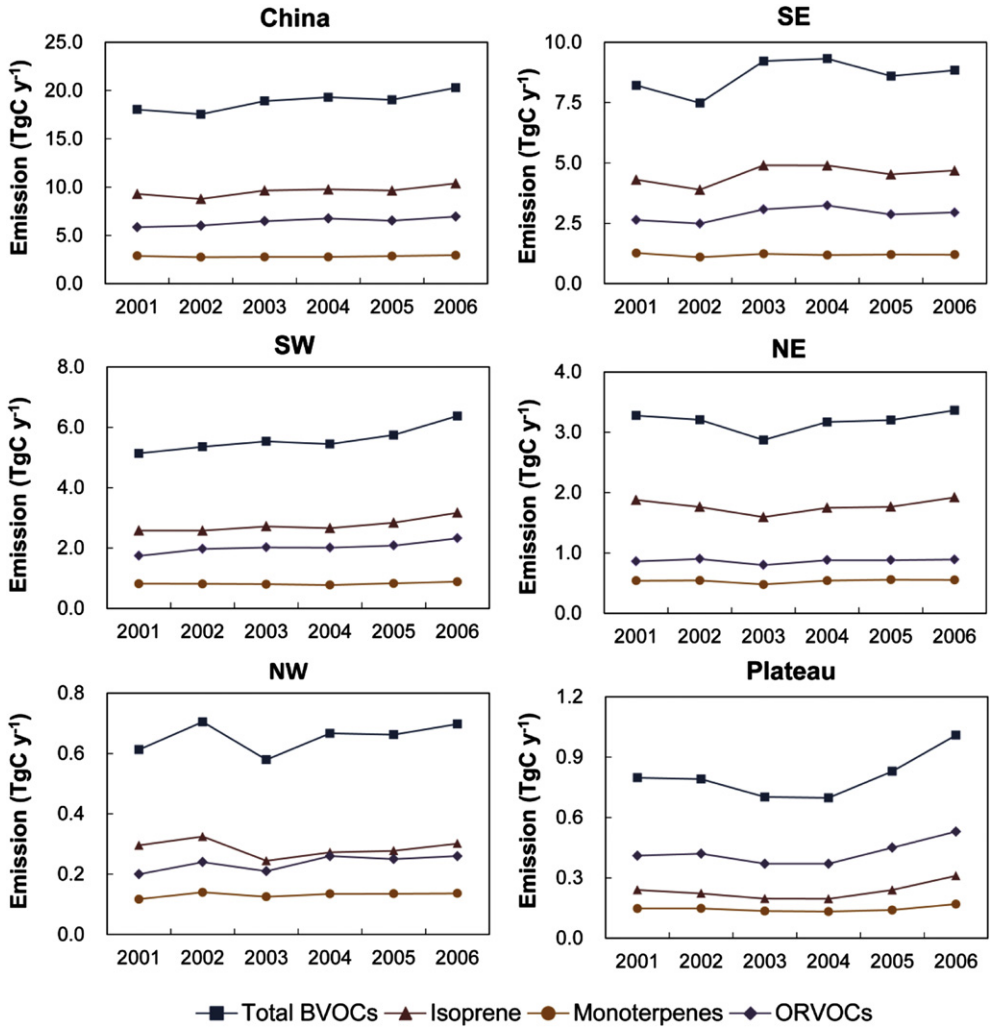

Fig. 5. Annual variations of isoprene, monoterpene, ORVOC, and total BVOC emissions in China and different regions simulated in ANNall.

In ANNmet, the interannual variations in meteorological fields can influence O_3 and SOA in two ways. First, changes in meteorological parameters influence chemical reactions, transport, and deposition of O_3 and SOA. Second, emissions of BVOCs vary with meteorological fields. We further separate these effects by performing two sensitivity simulations with the archived monthly BVOC emissions from ANNmet (Table 2):

(4) ANNmet_ATM: Sensitivity simulation for 2001–2006 to examine the sensitivity of O_3 and SOA to interannual variations in atmospheric conditions alone. We turn off MEGAN and use the year 2003 monthly BVOC emissions saved from the simulation ANNmet. Meteorological fields that drive the GEOS-Chem simulation are allowed to vary from 2001 to 2006.
(5) ANNmet_BVOCs: Sensitivity simulation for 2001–2006 to examine the interannual variations in O_3 and SOA as a result of the sensitivity of BVOC emissions to meteorological parameters. Year 2003 meteorological fields are used to drive the GEOS-Chem. The MEGAN module is turned off and monthly BVOC emissions of 2001–2006 saved from ANNmet are used for the simulation of O_3 and SOA.

In all the simulations mentioned above, anthropogenic emissions of O_3 precursors, aerosol precursors, and aerosols are fixed at the year 2003 levels. The simulated interannual variations will be presented for different regions in China, as defined in Fig. 2.

3. Simulated biogenic emissions in China

3.1. Spatial distributions of BVOC emissions

Fig. 3 shows the geographical distributions of annual biogenic emissions (10^{-3} kg C m^{-2} yr^{-1}) of isoprene, monoterpenes, and ORVOCs from simulation ANNall that are averaged over 2001–2006. The largest isoprene emissions are simulated over southeastern and southwestern China where significant amounts of evergreen and deciduous trees exist (Geng et al., 2011; Kesselmeier and Staudt, 1999). Large monoterpene emissions are found in southeastern and southwestern China where coniferous plants grow, and in northeastern China with needleleaf trees (Fig. 2). Emissions of ORVOCs are large mainly in southeastern China because of the broadleaf trees in the tropical region that have high ORVOC emission rates (Guenther et al., 1995; Klinger et al., 2002).

Simulated BVOC emissions averaged over 2001–2006 are shown in Table 3. The total biogenic emission in China is 18.85 Tg C yr^{-1}, in which isoprene, monoterpene, and ORVOC emissions account for 50.9% (9.59 Tg C yr^{-1}), 15.0% (2.83 Tg C yr^{-1}) and 34.1% (6.43 Tg C yr^{-1}), respectively. The annual isoprene emission simulated in this study is within the range of

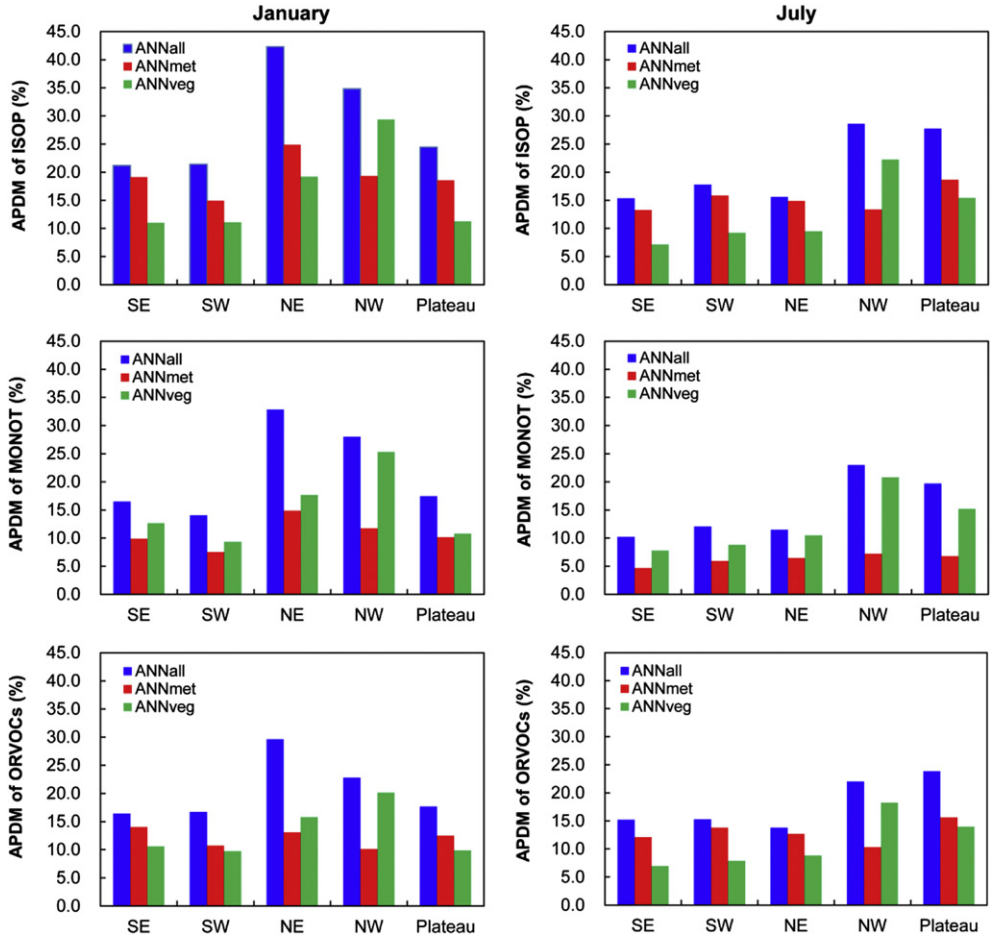

Fig. 6. The domain-averaged values of absolute percent departure from the mean (APDM, see Equation (4) in the text for the definition) for isoprene, monoterpene, and ORVOC emissions in January and July. Blue, red, and green columns represent APDM from simulations ANNall, ANNmet, and ANNveg, respectively. (For interpretation of the references to color in this figure legend, the reader is referred to the web version of this article.)

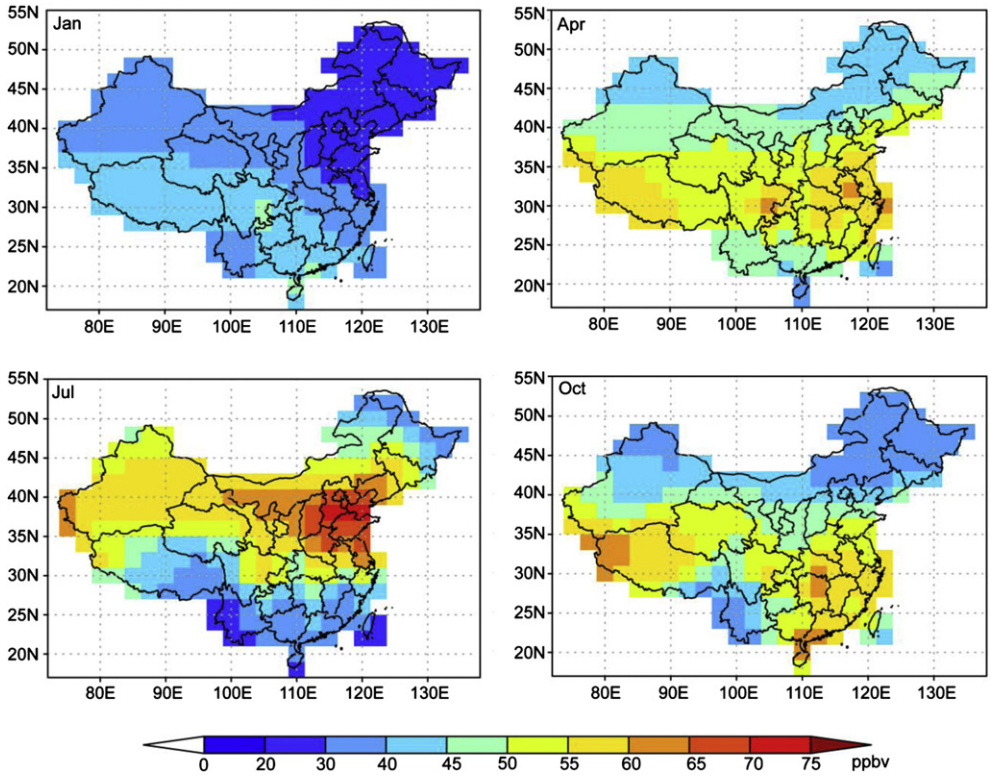

Fig. 7. Surface-layer concentrations (ppbv) of O_3 in January, April, July, and October averaged over years 2001–2006 of simulation ANNall.

4.1–15 Tg C yr^{-1} reported for China in Klinger et al. (2002). Our total emission of monoterpenes of 2.83 Tg C yr^{-1} is lower than the value of 3.5 Tg C yr^{-1} reported by Klinger et al. (2002) and 4.3 Tg C yr^{-1} reported by Guenther et al. (1995).

3.2. Seasonal variations

The BVOC emissions are the maximum in June–July–August (JJA); the 2001–2006 averages of BVOC emissions obtained from the simulation ANNall indicate that the total emission in China is 10.8 Tg C in JJA (57.3% of the annual emission) and 1.1 Tg C in December–January–February (DJF) (5.7% of the annual emission). Fig. 4 shows the ratios of isoprene, monoterpene, and ORVOC emissions to total BVOCs emission in January and July. In January, isoprene emissions generally account for 10–30% of total BVOCs in southern China, and the ratios of isoprene emissions to total BVOCs reach 30–50% in Yunnan province and the Pearl River Delta because of the dense distribution of tropical broadleaf trees that have high isoprene emission rates (Fig. 2). Monoterpene emissions contribute 20–40% to total BVOCs in January in most places in southern China. The ORVOC emissions dominate in January, accounting for 60–90% of total BVOCs in northern and northwestern China. The ratios of isoprene, monoterpene, and ORVOC emissions to total BVOCs in July show different patterns of distributions; isoprene emissions exceed 50% of total BVOCs in all regions with high biogenic emissions.

3.3. Interannual variations

The simulated interannual variations in emissions of isoprene, monoterpenes, and ORVOCs in ANNall are shown in Fig. 5 Over 2001–2006, the annual emissions of isoprene in China show an overall trend of increasing, but the interannual variations exhibit different behaviors in different regions. Annual isoprene emission in southeastern China has a minimum in 2002 and a maximum in 2003, with the maximum differing from the minimum by about 25%. The isoprene emissions in northeastern and northwestern China are the minimum in 2003 while those in Plateau are the smallest in 2004.

The interannual variations in simulated BVOC emissions can be quantified by mean absolute deviation (MAD) or absolute percent departure from the mean (APDM) defined as follows,

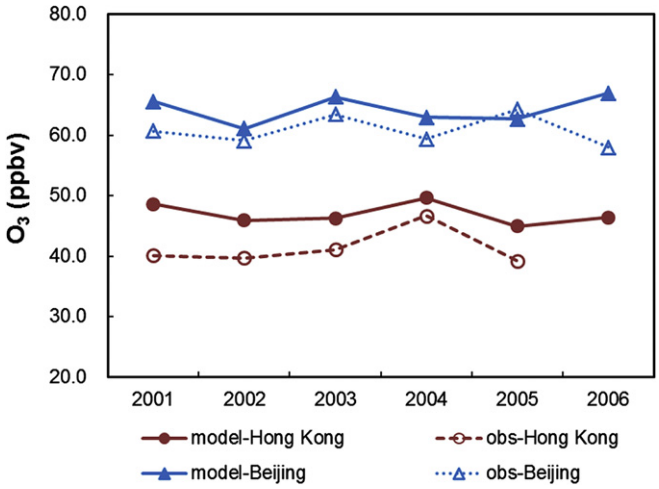

Fig. 8. Comparisons of the simulated surface-layer O_3 with measurements in Beijing and Hong Kong. Measurements in Beijing are the averages over July–September and over six stations in Beijing (Tang et al., 2009). The observations in Hong Kong are the annual means in Tung Chung site (Chan and Yao, 2008). Note the observed O_3 is defined as "$O_3 + NO_2$".

$$\mathrm{MAD}_m = \frac{1}{n}\sum_{i=1}^{n}\left|P_{i,m} - \frac{1}{n}\sum_{i=1}^{n}P_{i,m}\right| \quad (3)$$

$$\mathrm{APDM}_m = 100\% \times \mathrm{MAD}_m \Big/ \left(\frac{1}{n}\sum_{i=1}^{n}P_{i,m}\right) \quad (4)$$

where $P_{i,m}$ is the simulated monthly mean biogenic emission of a compound in the mth month of year i, and n is the number of years examined ($n = 6$ for years 2001–2006). Therefore MAD represents the absolute interannual variation and APDM represents the interannual variation relative to the average of biogenic emissions over the n years. For isoprene emissions obtained in simulation ANNall, the APDM values in January are in the range of 21–42% with the largest values (interannual variations) in northeastern and northwestern China, and those in July are in the range of 15–28% with the largest values in northwestern and the Plateau regions (Fig. 6). These interannual variations found in our work for isoprene are larger than the interannual variations of 15% reported by Arneth et al. (2011) for the northern high latitudes (60°–90°N). The roles of variations in meteorological and vegetation parameters can be quantified by simulations ANNmet and ANNveg, respectively. The APDM values of isoprene emissions in ANNmet are larger than those obtained in ANNveg by 3–8% in southeastern, southwestern, northeastern, and Plateau regions (Fig. 6), indicating that the interannual variations in isoprene are more dependent on variations in meteorological parameters than on changes in PFTs and LAIv, because isoprene emissions are parameterized to increase exponentially with temperature and have strong light dependence (Sakulyanontvittaya et al., 2008; Guenther et al., 2006).

The APDM values of monoterpene emissions are 14–32% in January and 10–21% in July (Fig. 6), which are generally smaller than those of isoprene emissions. The largest interannual variations of 18–32% are found in northeastern and northwestern China in January and in northwestern and Plateau regions in July. Although the large APDM values of monoterpenes occur in the same regions

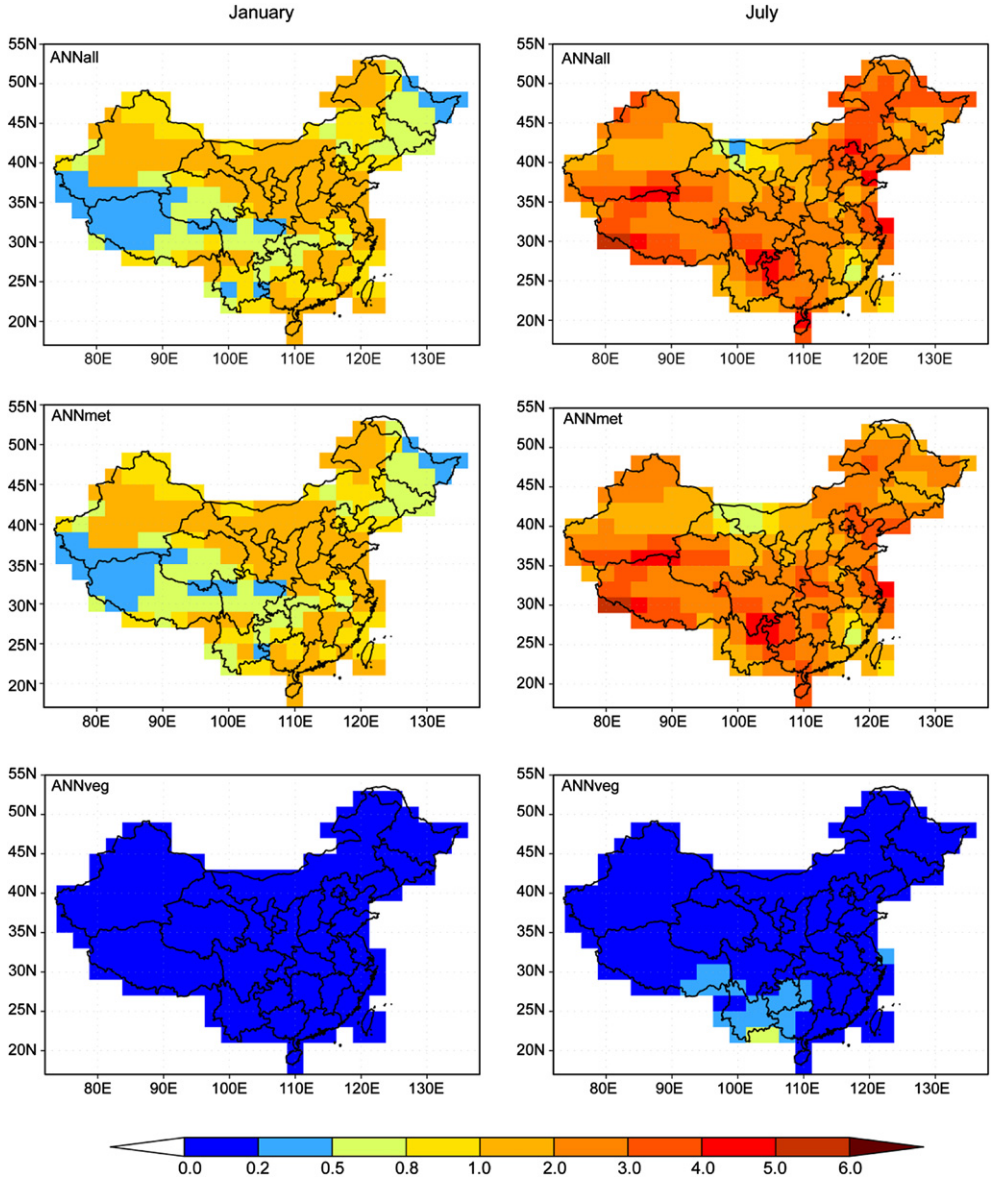

Fig. 9. Mean absolute deviation (MAD, see Equation (3) in the text for the definition, unit: ppbv) of surface-layer O_3 for January (left panels) and July (right panels) based on the simulated 2001–2006 O_3 concentrations in ANNall, ANNmet, and ANNveg.

as those of isoprene, changes in vegetation parameters play a more important role in influencing the interannual variations of monoterpenes, because APDM values obtained in ANNveg are larger than those obtained in ANNmet in all regions in China (Fig. 6). For ORVOCs, the APDM values in ANNall in January are about 15% in southern China where ORVOC emissions are the highest, and the values are in the range of 14–24% in July throughout China (Fig. 6).

4. Interannual variations in tropospheric ozone and SOA

4.1. Ozone

4.1.1. Simulated concentrations of ozone

Fig. 7 shows the simulated surface-layer concentrations of O_3 in January, April, July, October averaged over 2001–2006 of the ANNall simulation. In January, ozone concentrations in China are the lowest because of the weak photochemistry. Ozone concentrations of 40–50 ppbv are found in January over or near the Tibet Plateau as a result of the transport of O_3 from the stratosphere to troposphere (Wild and Akimoto, 2001). In April and October, O_3 concentrations increase throughout China as a result of enhanced photochemical production; concentrations of O_3 over 25°–40°N are in the range of 45–65 ppbv. The highest surface-layer O_3 concentrations of about 75 ppbv are found in July in Huabei Plain (110°–120°E, 35°–40°N), because of the strongest photochemistry as well as enhanced biogenic emissions. The industrialized Huabei Plain is generally VOCs-limited (Tang et al., 2011). Although biogenic emissions, temperature, and radiation are the highest in southeastern and southwestern China in July, O_3 concentrations over 20°–30°N are about 30–50 ppbv in this month, which can be explained by summer monsoon circulation that brings clean air to the regions (He et al., 2008).

4.1.2. Interannual variations in surface-layer ozone

The interannual variations of O_3 will be quantified in this section using the MAD and APDM values. We firstly evaluate the model's performance in simulating the interannual variations of O_3. Few sites in China have multi-year measurements of O_3; we examine

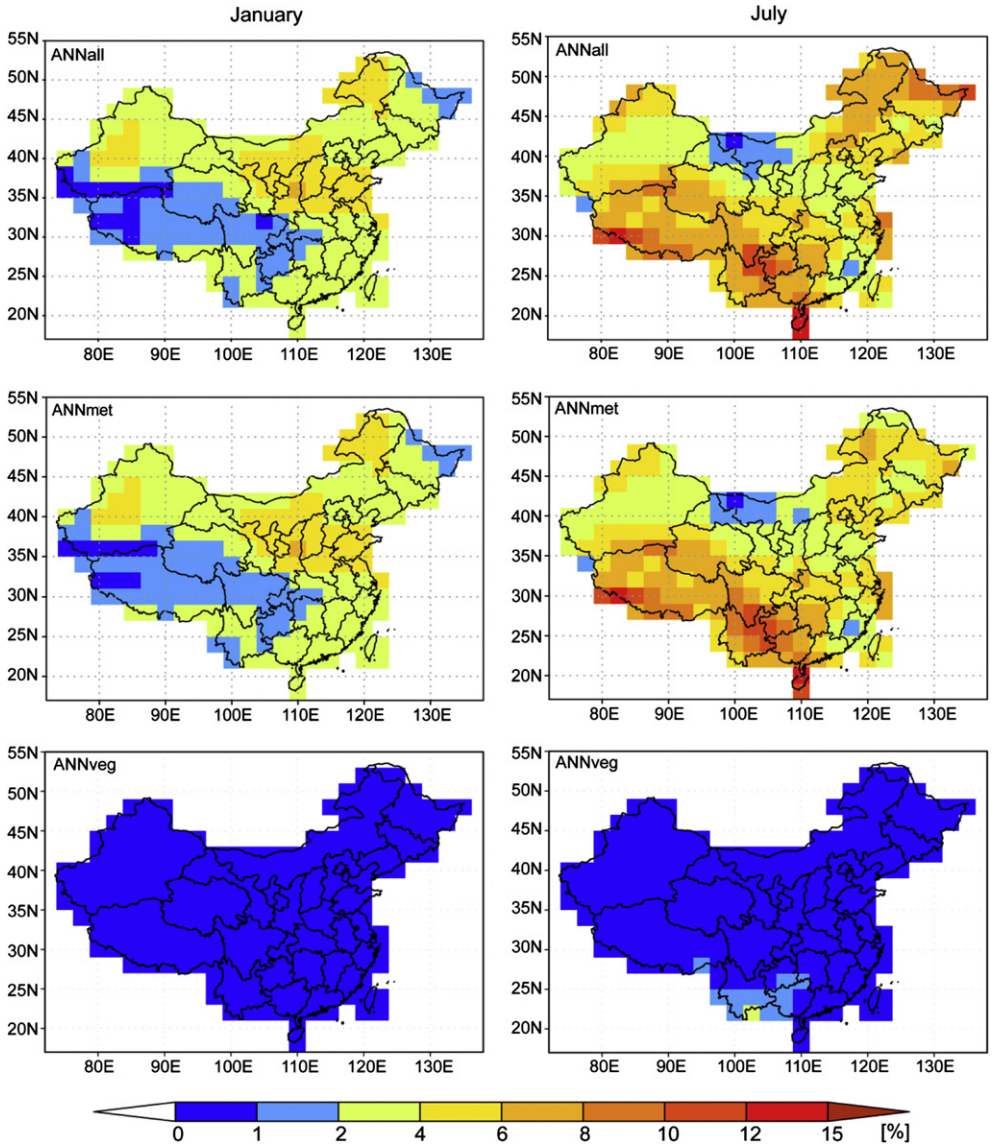

Fig. 10. Absolute percent departure from the mean (APDM, unit: %) of surface-layer O_3 for January (left panels) and July (right panels) based on the simulated 2001–2006 O_3 concentrations in ANNall, ANNmet, and ANNveg.

two representative sites, Beijing and Hong Kong, based on the measurements found in the literature. The measured and simulated surface-layer O_3 concentrations in Beijing for each year of 2001–2006 are the averages over July–September (Fig. 8). The simulated interannual variation of O_3 in Beijing agrees well with the observation over 2001–2005, but the simulated O_3 shows a peak in 2006 while the observed O_3 exhibits a minimum. Note that the anthropogenic emissions of O_3 precursors are fixed at the year 2003 levels in ANNall, which may lead to biases in simulation of O_3 of other years. Simulated O_3 concentrations in Beijing over 2001–2006 have a MAD value of about 2.0 ppbv, which is consistent with the deviation of the observations. The measured values of O_3 in Hong Kong are annual mean values (Fig. 8). The model can reproduce the interannual variation in Hong Kong, but tends to overestimate O_3 concentrations by 2–9 ppbv. The MAD value of the observed O_3 in Hong Kong over 2001–2005 is 2.4 ppbv, which is larger than the MAD value of 1.5 ppbv of the simulated O_3. These comparisons with the observations in Beijing and Hong Kong indicate that the model can capture reasonably well the interannual variations of O_3.

The interannual variations in O_3 in China are shown by MAD and APDM values for January and July (Figs. 9 and 10). In many places in China, the MAD values obtained in simulation ANNall are 0.8–3.0 ppbv in January and 3–5 ppbv in July. The highest values of APDM from ANNall are 4–8% over central, northeastern, and northwestern China in January, and 8–15% in southwestern and Plateau regions in July. These interannual variations in O_3 are significant as compared to the impacts of decadal-scale climate change on O_3. As shown by Jiang et al. (2008), over 2001–2051 the daily maximum 8-h O_3 concentrations in Houston, Texas increase by 2.6 ppbv as a result of the future climate change and the climate-induced increases in BVOCs under future A1B scenario. The significance of these interannual variations of O_3 can also be demonstrated when they are compared with the changes in O_3

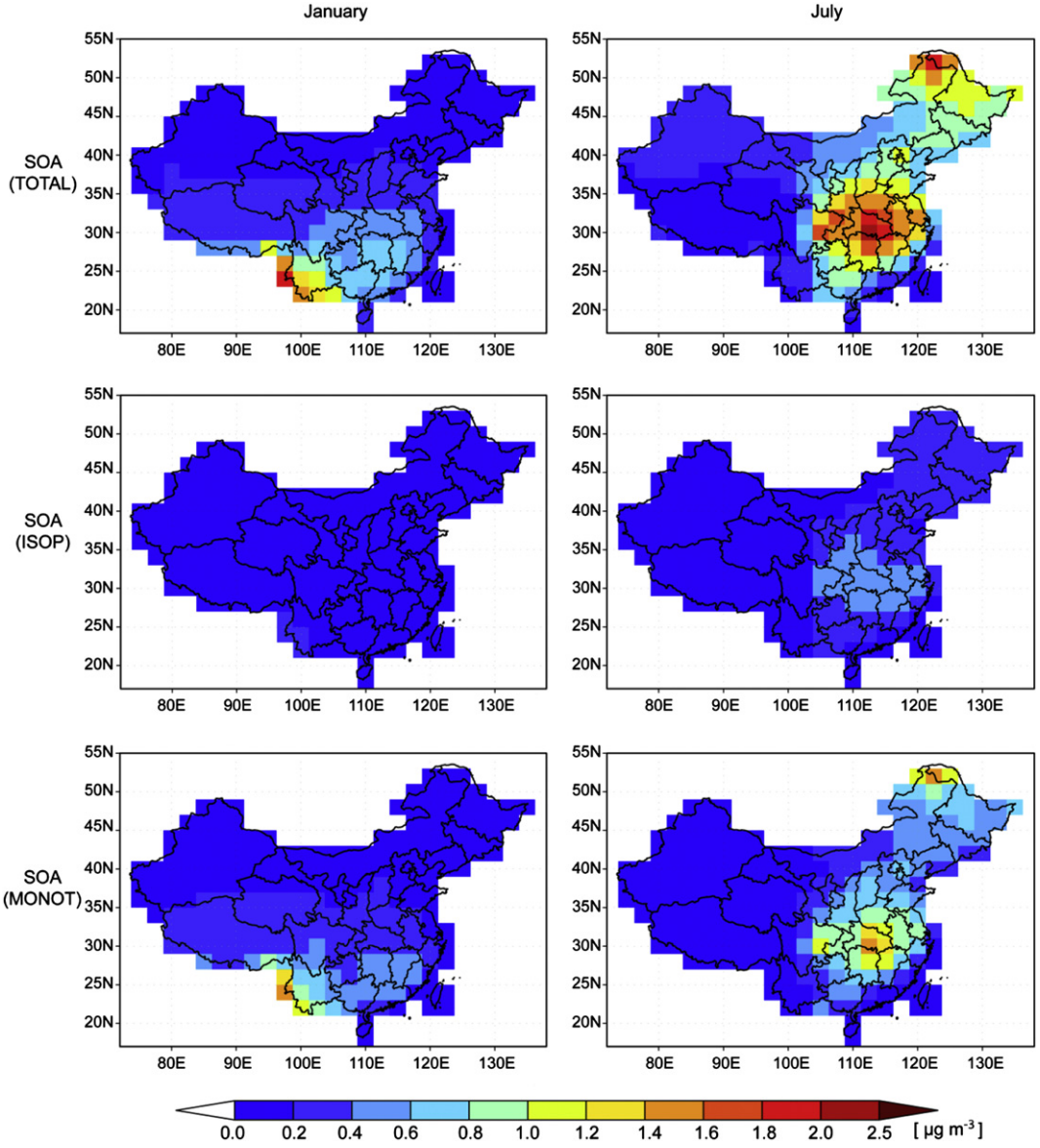

Fig. 11. Surface-layer concentrations (μg m^{-3}) of SOA in January and July averaged over years 2001–2006 of simulation ANNall. Top, middle, and bottom panels are total SOA (represents SOA from the oxidation of isoprene, monoterpenes, ORVOCs, benzene, toluene and xylen), SOA from the oxidation of isoprene, and SOA from the oxidation of monoterpenes, respectively.

concentrations by reductions in emissions. Sensitivity studies have shown that, in eastern China, reductions in NO_x or total VOCs (anthropogenic + biogenic VOCs) by 50% lead to changes in summer O_3 concentrations by 10–20% (Han et al., 2005). The pattern and magnitude of MAD and APDM values of O_3 obtained from ANNmet are similar to those obtained in ANNall, indicating that interannual variations in meteorological parameters are the major factors that influence the interannual variations of O_3.

4.2. SOA

4.2.1. Simulated concentrations of SOA

Fig. 11 shows simulated distributions of surface-layer SOA concentrations in January and July in ANNall from the oxidation of all VOCs (isoprene, monoterpenes, ORVOCs (including sesquiterpenes), benzene, toluene and xylene), isoprene, or monoterpenes. The distributions of SOA concentrations follow those of biogenic emissions (Fig. 3). In January, the largest SOA concentrations of 0.6–2.0 μg m^{-3} are simulated over southwestern and southeastern China, where biogenic emissions, temperature, and solar radiation are relatively high as compared with other regions. In July, the largest SOA concentrations of exceeding 2.0 μg m^{-3} are found in the lower and middle reaches of the Yangtze River and in northeastern China. Our simulated SOA levels in China agree with those obtained in studies of Henze and Seinfeld (2006) and Henze et al. (2008) using the GEOS-Chem model. It is also shown in Fig. 11 that SOA concentrations from monoterpenes are about twice the concentrations from the oxidation of isoprene.

4.2.2. Interannual variations in surface-layer SOA

The MAD (Fig. 12) and APDM (Fig. 13) values obtained in simulation ANNall show that SOA concentrations have large interannual variations. In January, MAD and APDM values are, respectively, 0.1–0.25 μg m^{-3} and 5–15% in southwestern China where SOA concentrations are the highest. In July, the highest MAD values are about 0.5 μg m^{-3} in southeastern and northeastern China, with APDM values of 10–25% in southeastern and 20–35% in northeastern regions. As can be seen from the MAD and APDM values from the simulations ANNmet and ANNveg, the interannual variations in meteorological parameters always have a dominant

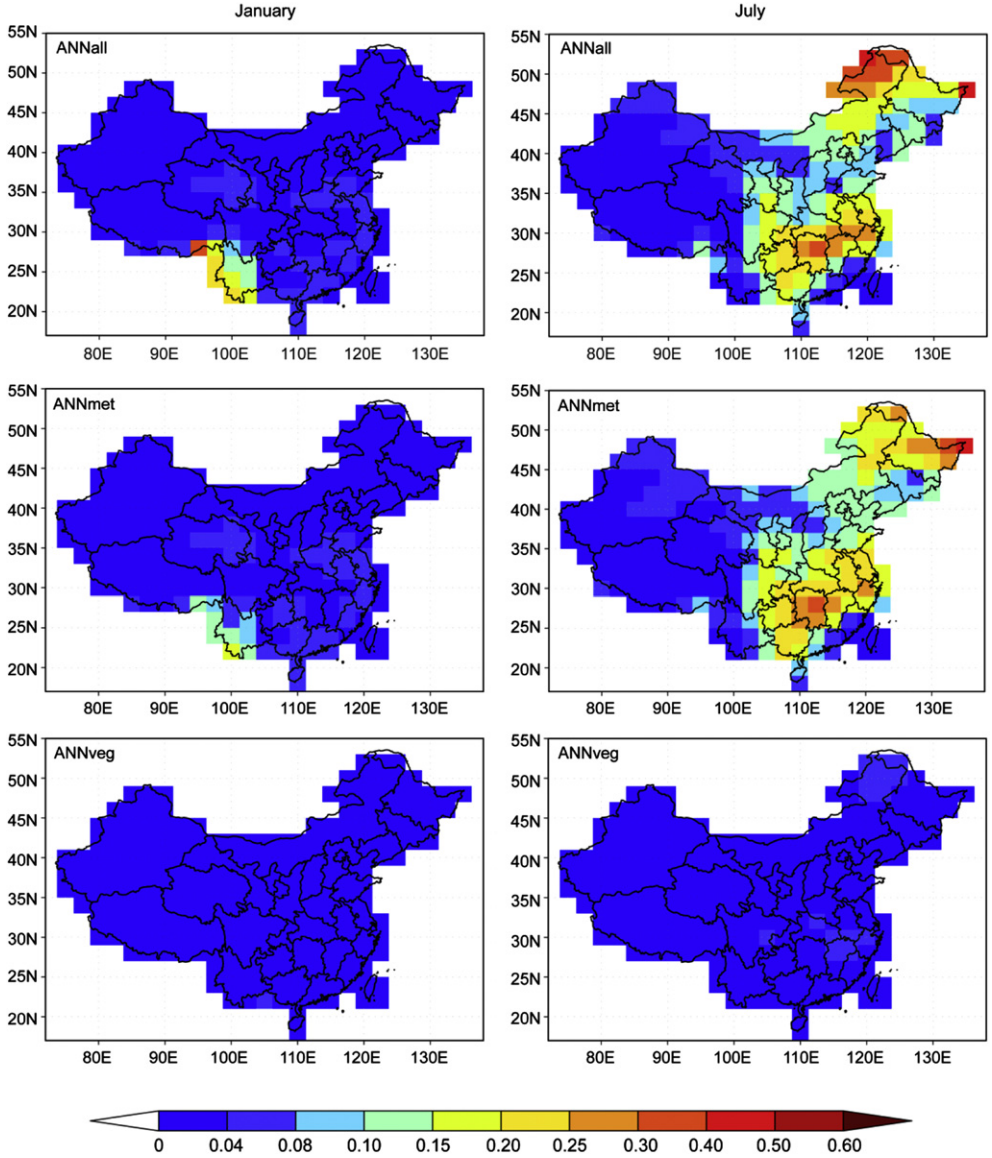

Fig. 12. Mean absolute deviation (MAD, unit: μg m^{-3}) of surface-layer SOA for January (left panels) and July (right panels) based on the simulated 2001–2006 SOA concentrations in ANNall, ANNmet, and ANNveg.

contribution to interannual variations of SOA. The variations in temperature influence SOA by changing biogenic emissions and shifting the gas-particle partitioning, and those in precipitation influence the wet deposition of SOA (Liao et al., 2006). The interannual variations in vegetation lead to APDM values of 2–5% in northeastern China and 5–10% in southeastern and southwestern China in July, which are smaller than the impacts of meteorological parameters but should be accounted for in SOA simulations. These interannual variations in SOA are significant as compared to the impacts of decadal-scale climate change on SOA. Jiang et al. (2010) predicted an increase in SOA concentrations by 5–26% in the United States as a result of climate change and the climate-induced BVOCs change over 2001–2051 under the A1B scenario.

5. Impacts of interannual variations in BVOC emissions on simulations of O_3 and SOA

The simulation ANNmet_ATM represents the interannual variations driven by changing atmospheric conditions alone (Table 2), from which we obtain the MAD values of 1–3 ppbv and APDM values of 3–8% for O_3 in all regions and seasons (Fig. 14). For comparison, the simulation ANNmet_BVOCs represents the interannual variations driven by interannual variations of BVOCs alone (Table 2). The MAD values of O_3 from ANNmet_BVOCs are smaller than 1 ppbv in all regions in both January and July, and the largest APDM value is about 2% in southwestern China in July.

The MAD and APDM values of simulated SOA in ANNmet_ATM and ANNmet_BVOCs are also compared in Fig. 14. In simulation ANNmet_ATM, the changes in chemical reactions, transport, and deposition have large impacts on SOA simulation, with APDM values of 12–24% in all regions in both January and July. In simulation ANNmet_BVOCs, the interannual variations in BVOCs have larger impacts on SOA in July than in January. In July, over the regions with the highest SOA concentrations, the interannual variation of SOA is about 2% in northeastern China as well as 5% in southeastern and southwestern China, as a result of the interannual variations of BVOC emissions alone.

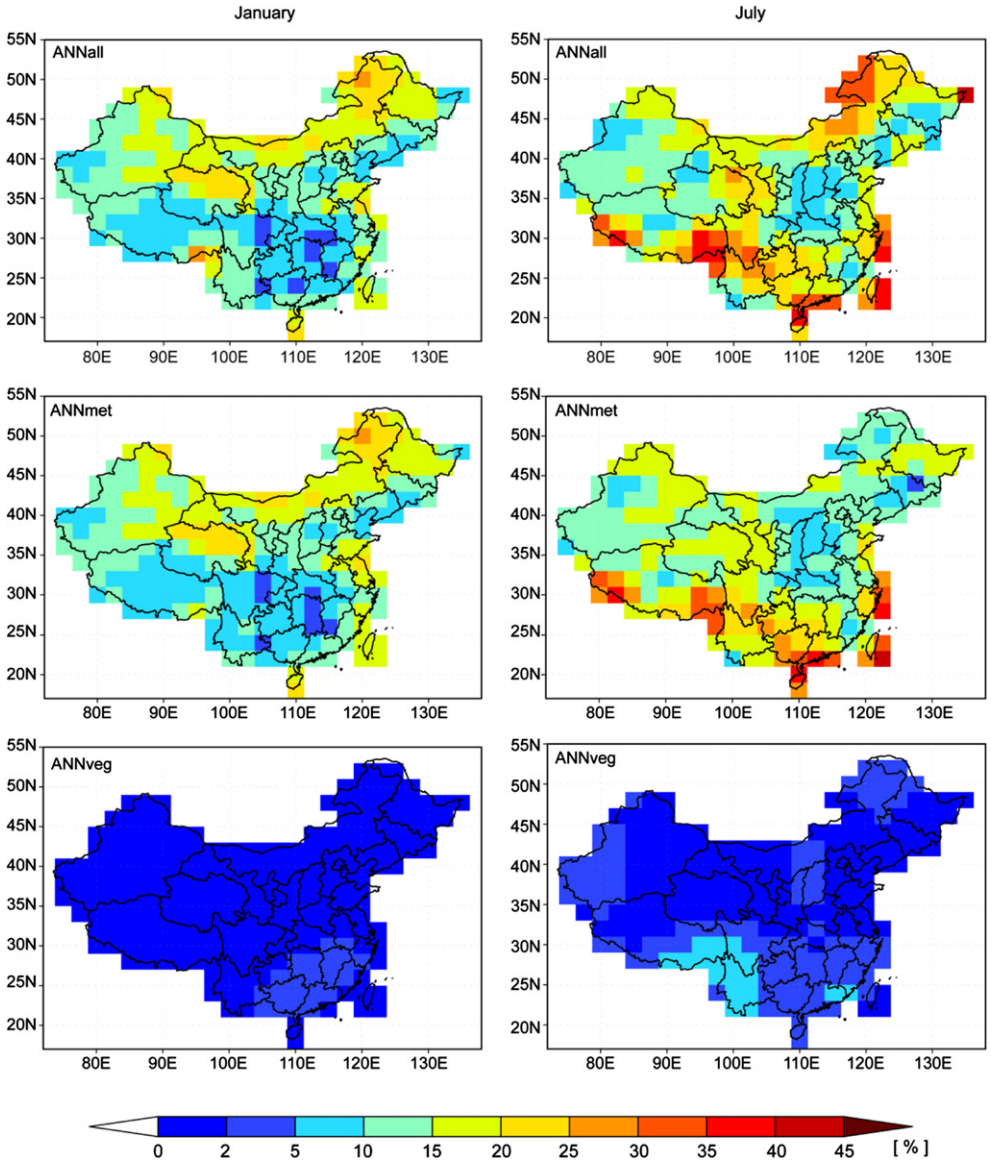

Fig. 13. Absolute percent departure from the mean (APDM, unit: %) of surface-layer SOA for January (left panels) and July (right panels) based on the simulated 2001–2006 SOA concentrations in ANNall, ANNmet, and ANNveg.

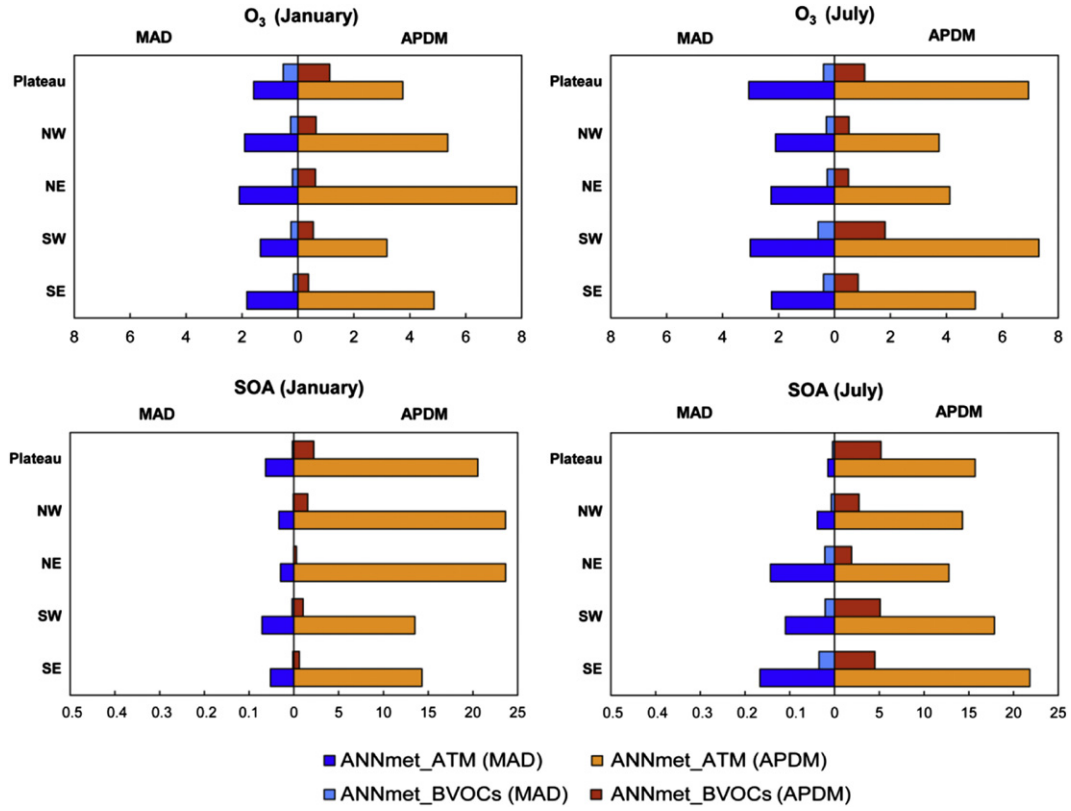

Fig. 14. Mean absolute deviation (MAD) and absolute percent departure from the mean (APDM, unit: %) obtained in sensitivity simulations ANNmet_ATM and ANNmet_BVOCs. The upper panels are for surface-layer O_3 and bottom panels are for surface-layer SOA. The unit of MAD is ppbv for O_3 and μg m^{-3} for SOA.

These model results suggest that changes in atmospheric conditions dominate the interannual variations of both O_3 and SOA, with much larger APDM values in SOA than in O_3 concentrations. The interannual variations in BVOCs alone can lead to 2–5% differences in simulated O_3 and SOA in summer. It should be noted that MAD and APDM values represent the averages over 2001–2006; the impacts of interannual variations in BVOC emissions for a specific year can be more significant than the magnitudes reported here. Furthermore, even if BVOC emissions are held constant, they are still a function of the reference year meteorology on which they are based.

6. Conclusions and discussion

We use the biogenic emission module MEGAN embedded within the global chemical transport model GEOS-Chem to estimate the interannual variations of BVOC emissions, O_3, and SOA over China for years 2001–2006. We have updated the land cover and leaf area index in China using the MODIS satellite measurements and developed a new classification of vegetation with 21 plant functional types to take into account different climatological conditions in China. We perform simulations ANNall, ANNmet, and ANNveg to identify the key parameters that influence the interannual variations of BVOCs, O_3, and SOA.

In simulation ANNall, with the combined effects of variations in meteorological parameters and land cover, the total BVOC emissions in China averaged over 2001–2006 is estimated to be 18.85 Tg C yr^{-1}, in which isoprene, monoterpenes, and ORVOCs account for 50.9%, 15.0%, and 34.1%, respectively. The highest biogenic emissions are found over southeastern, southwestern, and northeastern China.

We have defined two parameters, mean absolute deviation (MAD) and absolute percent departure from the mean (APDM), to quantify the interannual variations in BVOCs and concentrations of O_3 and SOA. Results of simulation ANNall show that isoprene emissions in China have large interannual variations; the APDM values in China are in the range of 21–42% in January and 15–28% in July. The APDM values of monoterpene emissions are generally smaller than those of isoprene emissions, with APDM values of 14–32% in January and 10–21% in July. Comparisons of simulation ANNall with ANNmet and ANNveg indicate that the interannual variations in isoprene emissions are more dependent on variations in meteorological parameters, whereas the interannual variations of monoterpene emissions are more sensitive to changes in PFTs and LAIv.

With respect to the interannual variations in O_3, the MAD values obtained in simulation ANNall are 0.8–3 ppbv in January and 3–5 ppbv in July. These interannual variations in O_3 are comparable in magnitude to the changes of O_3 of 1–10 ppbv by the decadal-scale climate change (Jacob and Winner, 2009). The interannual variations in meteorological parameters are the major factors that influence the variations of O_3, since the maximum APDM values from ANNveg are found to be small.

The simulation ANNall also shows that SOA concentrations have large interannual variations. Over the regions with highest SOA concentrations, the APDM values are 5–15% in southwestern China in January, and 10–25% in southeastern region and 20–35% in northeastern China in July. Again, the simulations ANNmet and ANNveg indicate that the interannual variations in meteorological parameters have a dominant contribution to interannual variations of SOA.

In ANNmet, meteorological parameters influence O_3 and SOA through changing atmospheric conditions (influencing chemical

reactions, transport, and deposition) and by the sensitivity of BVOCs to meteorological fields. These two effects are separated by sensitivity simulations ANNmet_ATM and ANNmet_BVOCs. Model results suggest that changes in atmospheric conditions dominate the interannual variations of both O_3 and SOA. Still, interannual variations in BVOCs alone can lead to 2–5% differences in simulated O_3 and SOA in summer.

There are some sources of uncertainties in our simulations, especially in the simulation of SOA. Results obtained here for SOA are based on SOA formation from absorptive partitioning. Recent studies have shown that the oxidation of primary gas-phase semivolatile organic compounds and the intermediate volatile organic compounds (Pye and Seinfeld, 2010), the heterogeneous uptake of dicarbonyls (Fu et al., 2008), and the aqueous reactions in clouds, fogs and aerosol water (Lim et al., 2010) may constitute potentially large sources of SOA. These issues suggest avenues for improvement in our future research.

Acknowledgments

This work was supported by the Chinese Academy of Sciences Strategic Priority Research Program Grant No. XDA05100503, the National Natural Science Foundation of China under grants 40825016 and 41021004, the special funding in atmospheric science GYHY200906020. The MODIS products are obtained through the online Data Pool at the NASA Land Processes Distributed Active Archive Center (LP DAAC).

References

Alexander, B., Park, R.J., Jacob, D.J., Li, Q.B., Yantosca, R.M., Savarino, J., Lee, C.C.W., Thiemens, M.H., 2005. Sulfate formation in sea-salt aerosols: constraints from oxygen isotopes. J. Geophys. Res. 110, D10307. http://dx.doi.org/10.1029/2004JD005659.

Arneth, A., Schurgers, G., Hickler, T., Miller, P.A., 2008. Effects of species composition, land surface cover, CO_2 concentration and climate on isoprene emissions from European forests. Plant Biol. 10, 150–162.

Arneth, A., Schurgers, G., Lathiere, J., Duhl, T., Beerling, D.J., Hewitt, C.N., Martin, M., Guenther, A., 2011. Global terrestrial isoprene emission models: sensitivity to variability in climate and vegetation. Atmos. Chem. Phys. 11, 8037–8052.

Bai, J.H., Baker, B., Liang, B.S., Greenberg, J., Guenther, A., 2006. Isoprene and monoterpene emissions from an Inner Mongolia grassland. Atmos. Environ. 40, 5753–5758.

Bey, I., Jacob, D.J., Yantosca, R.M., Logan, J.A., Field, B.D., Fiore, A.M., Li, Q., Liu, H.Y., Mickley, L.J., Schultz, M.G., 2001. Global modeling of tropospheric chemistry with assimilated meteorology: model description and evaluation. J. Geophys. Res. 106, 23073–23095. http://dx.doi.org/10.1029/2001JD000807.

Bonan, G.B., Levis, S., Kergoat, L., Oleson, K.W., 2002. Landscapes as patches of plant functional types: an integrating concept for climate and ecosystem models. Global. Biogeochem. Cycles 16, 1021. http://dx.doi.org/10.1029/2000GB001360.

Carslaw, K.S., Boucher, O., Spracklen, D.V., Mann, G.W., Rae, J.G.L., Woodward, S., Kulmala, M., 2010. A review of natural aerosol interactions and feedbacks within the Earth system. Atmos. Chem. Phys. 10, 1701–1737.

Chan, C.K., Yao, X., 2008. Air pollution in mega cities in China. Atmos. Environ. 42 (1), 1–42.

CNIS, 1998. Names and Codes for Climate Regionalization in China-Climatic Zones and Climatic Regions (GB/T 17297-1998) (in Chinese).

Curci, G., Beekmann, M., Vautard, R., Smiatek, G., Steinbrecher, R., Theloke, J., Friedrich, R., 2009. Modelling study of the impact of isoprene and terpene biogenic emissions on European ozone levels. Atmos. Environ. 43, 1444–1455.

Fairlie, T.D., Jacob, D.J., Park, R.J., 2007. The impact of transpacific transport of mineral dust in the United States. Atmos. Environ. 41, 1251–1266.

Friedl, M.A., Sulla-Menashe, D., Tan, B., Schneider, A., Ramankutty, N., Sibley, A., Huang, X., 2010. MODIS collection 5 global land cover: algorithm refinements and characterization of new datasets. Remote Sens. Environ. 114, 168–182.

Fu, T.M., Jacob, D.J., Wittrock, F., Burrows, J.P., Vrekoussis, M., Henze, D.K., 2008. Global budgets of atmospheric glyoxal and methylglyoxal, and implications for formation of secondary organic aerosols. J. Geophys. Res. 113, D15303. http://dx.doi.org/10.1029/2007JD009505.

Geng, F., Tie, X., Guenther, A., Li, G., Cao, J., Harley, P., 2011. Effect of isoprene emissions from major forests on ozone formation in the city of Shanghai, China. Atmos. Chem. Phys. 11, 10449–10459.

Guenther, A., Hewitt, C.N., Erickson, D., Fall, R., Geron, C., Graedel, T., Harley, P., Klinger, L., Lerdau, M., Mckay, W.A., Pierce, T., Scholes, B., Steinbrecher, R., Tallamraju, R., Taylor, J., Zimmerman, P., 1995. A global model of natural volatile organic compound emissions. J. Geophys. Res. 100, 8873–8892. http://dx.doi.org/10.1029/94JD02950.

Guenther, A., Karl, T., Harley, P., Wiedinmyer, C., Palmer, P.I., Geron, C., 2006. Estimates of global terrestrial isoprene emissions using MEGAN (Model of Emissions of Gases and Aerosols from Nature). Atmos. Chem. Phys. 6, 3181–3210.

Han, Z., Ueda, H., Matsuda, K., 2005. Model study of the impact of biogenic emission on regional ozone and the effectiveness of emission reduction scenarios over eastern China. Tellus 57, 12–27.

He, Y.J., Uno, I., Wang, Z.F., Pochanart, P., Li, J., Akimoto, H., 2008. Significant impact of the East Asia monsoon on ozone seasonal behavior in the boundary layer of Eastern China and the west Pacific region. Atmos. Chem. Phys. 8, 7543–7555.

Heald, C.L., Henze, D.K., Horowitz, L.W., Feddema, J., Lamarque, J.F., Guenther, A., Hess, P.G., Vitt, F., Seinfeld, J.H., Goldstein, A.H., Fung, I., 2008. Predicted change in global secondary organic aerosol concentrations in response to future climate, emissions, and land use change. J. Geophys. Res. 113, 1–16. http://dx.doi.org/10.1029/2007JD009092.

Henze, D.K., Seinfeld, J.H., 2006. Global secondary organic aerosol from isoprene oxidation. Geophys. Res. Lett. 33, L09812. http://dx.doi.org/10.1029/2006GL025976.

Henze, D.K., Seinfeld, J.H., Ng, N.L., Kroll, J.H., Fu, T.M., Jacob, D.J., Heald, C.L., 2008. Global modeling of secondary organic aerosol formation from aromatic hydrocarbons: high- vs. low-yield pathways. Atmos. Chem. Phys. 8, 2405–2420.

IPCC, 2007. Climate change 2007: the physical science basis. Contribution of working group I to the fourth assessment report of the intergovernmental panel on climate change. In: Solomon, S., et al. (Eds.). Cambridge University Press, Cambridge, United Kingdom and New York, pp. 1–996.

Jacob, D.J., Winner, D.A., 2009. Effect of climate change on air quality. Atmos. Environ. 43, 51–63.

Jiang, X.Y., Wiedinmyer, C., Chen, F., Yang, Z.L., Lo, J.C.F., 2008. Predicted impacts of climate and land use change on surface ozone in the Houston, Texas, area. J. Geophys. Res. 113. http://dx.doi.org/10.1029/2008JD009820

Jiang, X.Y., Yang, Z.L., Liao, H., Wiedinmyer, C., 2010. Sensitivity of biogenic secondary organic aerosols to future climate change at regional scales an online coupled simulation. Atmos. Environ. 44, 4891–4907.

Kanakidou, M., Tsigaridis, K., 2007. Secondary organic aerosol importance in the future atmosphere. Atmos. Environ. 41, 4682–4692.

Kesselmeier, J., Staudt, M., 1999. Biogenic volatile organic compounds (VOC): an overview on emission, physiology and ecology. J. Atmos. Chem. 33, 23–88.

Klinger, L.F., Li, Q.J., Guenther, A.B., Greenberg, J.P., Baker, B., Bai, J.H., 2002. Assessment of volatile organic compound emissions from ecosystems of China. J. Geophys. Res. 107, 4603. http://dx.doi.org/10.1029/2001JD001076.

Lathière, J., Hewitt, C.N., Beerling, D.J., 2010. Sensitivity of isoprene emissions from the terrestrial biosphere to 20th century changes in atmospheric CO_2 concentration, climate, and land use. Global. Biogeochem. Cycles 24, GB1004. http://dx.doi.org/10.1029/2009GB003548.

Lathiere, J., Hauglustaine, D.A., Friend, A.D., De Noblet-Ducoudre, N., Viovy, N., Folberth, G.A., 2006. Impact of climate variability and land use changes on global biogenic volatile organic compound emissions. Atmos. Chem. Phys. 6, 2129–2146.

Levis, S., Wiedinmyer, C., Bonan, G.B., Guenther, A., 2003. Simulating biogenic volatile organic compound emissions in the community climate system model. J. Geophys. Res. 108 (D21), 4659. http://dx.doi.org/10.1029/2002JD003203.

Liao, H., Chen, W.T., Seinfeld, J.H., 2006. Role of climate change in global predictions of future tropospheric ozone and aerosols. J. Geophys. Res. 111, D12304. http://dx.doi.org/10.1029/2005JD006852.

Liao, H., Henze, D.K., Seinfeld, J.H., Wu, S.L., Mickley, L.J., 2007. Biogenic secondary organic aerosol over the United States: comparison of climatological simulations with observations. J. Geophys. Res. 112, D06201. http://dx.doi.org/10.1029/2006JD007813.

Lim, Y.B., Tan, Y., Perri, M.J., Seitzinger, S.P., Turpin, B.J., 2010. Aqueous chemistry and its role in secondary organic aerosol (SOA) formation. Atmos. Chem. Phys. 10, 10521–10539.

Lin, J.T., Patten, K.O., Hayhoe, K., Liang, X.Z., Wuebbles, D.J., 2008. Effects of future climate and biogenic emissions changes on surface ozone over the United States and China. J. Appl. Meteorol. Clim. 47, 1888–1909.

Liu, H., Jacob, D.J., Bey, I., Yantosca, R.M., 2001. Constraints from 210Pb and 7Be on wet deposition and transport in a global three-dimensional chemical tracer model driven by assimilated meteorological fields. J. Geophys. Res. 106, 12109–12128. http://dx.doi.org/10.1029/2000JD900839.

Myneni, R.B., Hoffman, S., Knyazikhin, Y., Privette, J.L., Glassy, J., Tian, Y., Wang, Y., Song, X., Zhang, Y., Smith, G.R., Lotsch, A., Friedl, M., Morisette, J.T., Votava, P., Nemani, R.R., Running, S.W., 2002. Global products of vegetation leaf area and fraction absorbed PAR from year one of MODIS data. Remote Sens. Environ. 83, 214–231.

Nozière, B., González, N.J.D., Borg-Karlson, A.-K., Pei, Y., Redeby, J.P., Krejci, R., Dommen, J., Prevot, A.S.H., Anthonsen, T., 2011. Atmospheric chemistry in stereo: a new look at secondary organic aerosols from isoprene. Geophys. Res. Lett. 38, L11807. http://dx.doi.org/10.1029/2011GL047323.

Olivier, J.G.J., Berdowski, J.J.M., 2001. Global emissions sources and sinks. In: Berdowski, J., et al. (Eds.), The Climate System. A.A. Balkema Publishers/Swets & Zeitlinger Publishers, Lisse, The Netherlands, pp. 33–78.

Olson, C.E., 1992. World Ecosystems (WE1.4). In: Digital Raster Data on a 10-minute Geographic 1080 × 2160 Grid, Global Ecosystems Database, Version 1.0: Disc A. National Geophysical Data Center.

Park, R.J., Jacob, D.J., Chin, M., Martin, R.V., 2003. Sources of carbonaceous aerosols over the United States and implications for natural visibility. J. Geophys. Res. 108, 4355. http://dx.doi.org/10.1029/2002JD003190.

Park, R.J., Jacob, D.J., Field, B.D., Yantosca, R.M., Chin, M., 2004. Natural and transboundary pollution influences on sulfate-nitrate-ammonium aerosols in the United States: implications for policy. J. Geophys. Res. 109, D15204. http://dx.doi.org/10.1029/2003JD004473.

Piccot, S.D., Watson, J.J., Jones, J.W., 1992. A global inventory of volatile organic compound emissions from anthropogenic sources. J. Geophys. Res. 97, 9897–9912. http://dx.doi.org/10.1029/92JD00682.

Pye, H.O.T., Liao, H., Wu, S., Mickley, L.J., Jacob, D.J., Henze, D.K., Seinfeld, J.H., 2009. Effect of changes in climate and emissions on future sulfate-nitrate-ammonium aerosol levels in the United States. J. Geophys. Res. 114, D01205. http://dx.doi.org/10.1029/2008JD010701.

Pye, H.O.T., Seinfeld, J.H., 2010. A global perspective on aerosol from low-volatility organic compounds. Atmos. Chem. Phys. 10, 4377–4401.

Sakulyanontvittaya, T., Duhl, T., Wiedinmyer, C., Helmig, D., Matsunaga, S., Potosnak, M., Milford, J., Guenther, A., 2008. Monoterpene and sesquiterpene emission estimates for the United States. Environ. Sci. Technol. 42 (5), 1623–1629. http://dx.doi.org/10.1021/es702274e.

Sanderson, M.G., Jones, C.D., Collins, W.J., Johnson, C.E., Derwent, R.G., 2003. Effect of climate change on isoprene emissions and surface ozone levels. Geophys. Res. Lett. 30, 1936. http://dx.doi.org/10.1029/2003GL017642.

Schurgers, G., Arneth, A., Holzinger, R., Goldstein, A.H., 2009. Process-based modelling of biogenic monoterpene emissions combining production and release from storage. Atmos. Chem. Phys. 9, 3409–3423.

Steiner, A., Luo, C., Huang, Y., Chameides, W.L., 2002. Past and present-day biogenic volatile organic compound emissions in East Asia. Atmos. Environ. 36, 4895–4905.

Streets, D.G., Zhang, Q., Wang, L., He, K., Hao, J., Wu, Y., Tang, Y., Carmichael, G.R., 2006. Revisiting China's CO emissions after the transport and chemical evolution over the Pacific (TRACE-P) mission: synthesis of inventories, atmospheric modeling, and observations. J. Geophys. Res. 111, D14306. http://dx.doi.org/10.1029/2006JD007118.

Tang, G., Li, X., Wang, Y., Xin, J., Ren, X., 2009. Surface ozone trend details and interpretations in Beijing, 2001–2006. Atmos. Chem. Phys. 9, 8813–8823.

Tang, G., Wang, Y., Li, X., Ji, D., Gao, X., 2011. Spatial-temporal variations of surface ozone and ozone control strategy for Northern China. Atmos. Chem. Phys. Discuss. 11, 26057–26109.

Tsigaridis, K., Lathiere, J., Kanakidou, M., Hauglustaine, D.A., 2005. Naturally driven variability in the global secondary organic aerosol over a decade. Atmos. Chem. Phys. 5, 1891–1904.

Wiedinmyer, C., Sakulyanontvittaya, T., Guenther, A., 2007. MEGAN FORTRAN Code V2.04 User Guide. http://acd.ucar.edu/~guenther/MEGAN/MEGAN.htm.

Wiedinmyer, C., Tie, X., Guenther, A., Neilson, R., Granier, C., 2006. Future changes in biogenic isoprene emissions: how might they affect regional and global atmospheric chemistry? Earth Interact 10, 1–19.

Wild, O., Akimoto, H., 2001. Intercontinental transport of ozone and its precursors in a three-dimensional global CTM. J. Geophys. Res. 106, 27729–27744. http://dx.doi.org/10.1029/2000JD000123.

Wu, S.L., Mickley, L.J., Kaplan, J.O., Jacob, D.J., 2012. Impacts of changes in land use and land cover on atmospheric chemistry and air quality over the 21st century. Atmos. Chem. Phys. 12, 1597–1609.